Supporting Information

"A Metastable Cu(I)-Niobate Semiconductor with a Low Temperature Nanoparticle-Mediated Synthesis"

Jonglak Choi, Nacole King, and Paul A. Maggard*
Department of Chemistry, North Carolina State University, Raleigh, NC 27695-8204

Table S1. Selected crystal and refinement data for $Cu_2Nb_8O_{21}$.

Formula	$Cu_2Nb_8O_{21}$
Formula Weight (*g/mol*)	1206.36
Space Group, *Z*	*C2/m* (12), 2
Crystal System	Monoclinic
Temperature (K)	223(2)
Unit Cell (Å), *a*	10.5325(2)
b	6.4306(1)
c	10.1730(2)
β (^{o})	100.212(1)
V (Å^3)	678.11(2)
ρ (g/cm^3)	5.908
μ, (mm^{-1})	9.698
Data/restraints/parameters	2420/0/86
[a] R_1, wR_2 [I>2σ(I)]	0.0357, 0.0738
Goodness-of-Fit	1.009

[a] $R_f = \Sigma(|F_o-F_c|)/\Sigma F_o$; $R_w = [\Sigma(w(F_o^2-F_c^2)^2) / (\Sigma(F_o^2)^2)]^{1/2}$; $w = \sigma_F^{-2}$.

Table S2. Selected interatomic distances and calculated bond valence sums[28,29] for $Cu_2Nb_8O_{21}$.

Bond Distance Type		Distance (Å)		Bond Distance Type		Distance (Å)	
Nb1	– O(1)	2.002(3)		Nb3	– O(1)	2.032(3)	
	– O(2)	1.890(3)			– O(3)	1.8834(3)	
	– O(5)	2.074(2)	×2		– O(4)	2.063(2)	×2
	– O(5)	2.100(2)	×2		– O(7)	2.077(3)	
	– O(7)	2.114(3)			– O(8)	2.073(2)	×2
Bond Valence Sum		5.1		**Bond Valence Sum**		5.2	
Nb2	– O(4)	2.010(2)	×2	Nb4	– O(2)	2.229(3)	
	– O(5)	2.022(2)	×2		– O(4)	2.090(2)	×2
	– O(6)	2.185(2)			– O(6)	1.765(2)	
	– O(8)	1.988(2)	×2		– O(7)	2.054(3)	
Bond Valence Sum		5.3			– O(8)	2.108(2)	×2
				Bond Valence Sum		5.2	
				Cu	– O(1)	2.095(2)	×2
					– O(2)	2.095(2)	×2
				Bond Valence Sum		0.74	

Description of Mott-Schottky Measurements and Calculations.

Mott-Schottky measurements were performed using the AC electrochemical impedance method with an AC amplitude of 5 mV at an applied frequency of 9 kHz at pH 12 on a PARSTAT 23263 potentiostat-galvanostat instrument.

The space charge capacitance C may vary with the applied potential over the depletion layer as determined by the Mott-Schottky equation for a *p*-type semiconductor:

$$\frac{1}{C^2} = \left(\frac{2}{e\varepsilon_o \varepsilon_r N_A A^2}\right)\left(-V + V_{fb} - \frac{kT}{e}\right)$$

Where e is the electron charge, ε_r is the dielectric constant, ε_o is the permittivity of a vacuum, N_A is the acceptor density, V is the applied bias, V_{fb} is the flatband potential, k is the Boltzmann constant, T is room temperature, and A is the surface area of the film in contact with the electrolyte.

Therefore a plot of C^{-2} versus V should yield a straight line with a slope than can be used to determine N_A. Slope = $(2/e\varepsilon_r\varepsilon_0 N_A A^2)$; the value for ε_r was chosen as ~10, A = 0.125 m^2, ε_0 = 8.8541×10^{-12} Fm^{-1}, and e = 1.602×10^{-19} C

Slope from trial 1 (-8.80×10^6 $F^{-2}V^{-1}$) and from trial 2 (-4.23×10^7 $F^{-2}V^{-1}$)

Thus, an N_A from trial 1 ($1.03 \times 10^{18}cm^{-3}$) and trial 2 ($2.13 \times 10^{17}cm^{-3}$) was obtained at 9 kHz.

Using the above Mott-Schottky equation, the flatband potential is determined from the intercept with the *x*-axis on the linear plot of C^{-2} versus V and converted from SCE to RHE. The *x*-axis intercept for trial 1 was +0.032V vs. RHE and for trial 2 was +0.022V vs. RHE at a pH = 12.

Hence, V_{fb} for trial 1 is (.058 V) and for trial 2 (+.048 V).

The energetic position of the valence band (E_v) is determined from the equation for a *p*-type semiconductor:

$E_v = V_{fb}$ - kT ln (N_A/N_V) where Nv is the effective density of states (typically ~10^{19}) at the valence band edge.

Hence, E_v for trial 1 (0.118 V) and trial 2 (0.147 V).

Therefore, the position of the conduction can determined when the bandgap (1.65 eV) is subtracted from the valence band. The conduction band position trial 1 (-1.53 V) and trial 2 (-1.50 V) versus RHE at pH = 12.

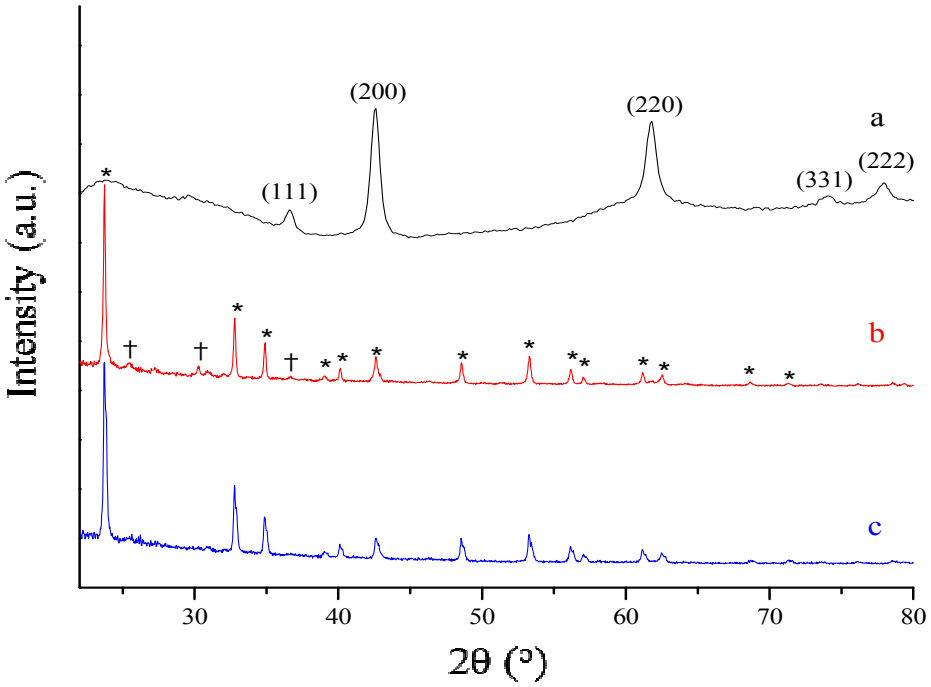

Figure S1. Powder X-ray plots of a) prepared nano Li_3NbO_4 (indexed from ICSD-PDF # 97-010-9053); b) heat treated a at 400 ^oC for 2 days in air; c) heat treatment of (b) at 400 ^oC for 5 days in air. Note * = $LiNbO_3$ (JCPDS # 1-74-2236), † = $LiNb_3O_8$ (JCPDS # 1-70-1566).

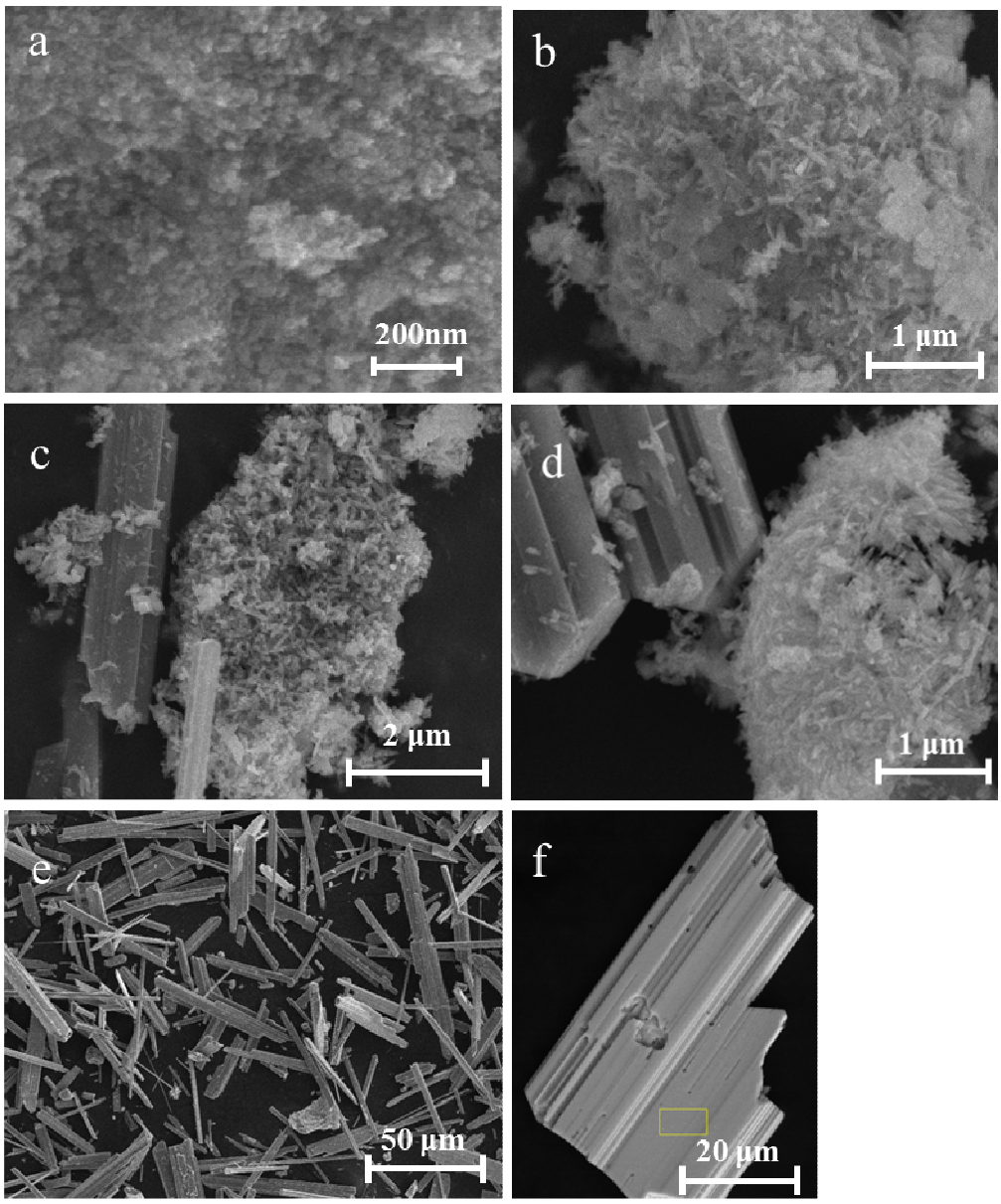

Figure S2. SEM images of the $Cu_2Nb_8O_{21}$ particles heated to 450 ^oC for a) 30minutes, b) 1hr, c) 5hr, d) 8hr, e) 1 day, and f) a higher magnification on one of the crystals in (e).

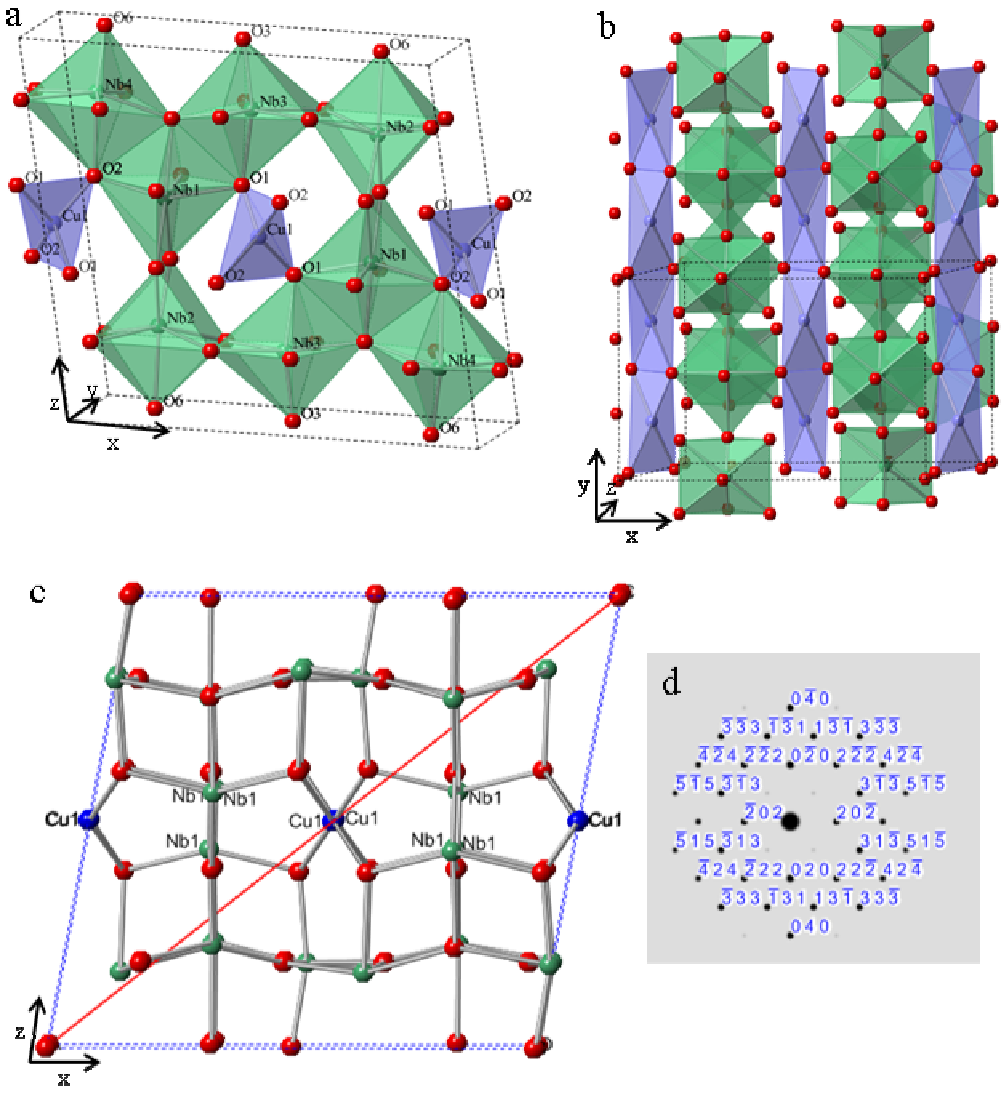

Figure S3. Polyhedral structural view of $Cu_2Nb_8O_{21}$ (a and b); c, unit-cell structural view with the [101] zone axis labeled (red line); d) simulated transmission electron diffraction pattern for the [101] zone axis. Note: red, green, blue spheres represent oxygen, niobium, copper, respectively, and green and purple polyhyedra indicate the coordination of copper and niobium to oxygen, respectively. The blue numbers in d) are the labeled miller indices.

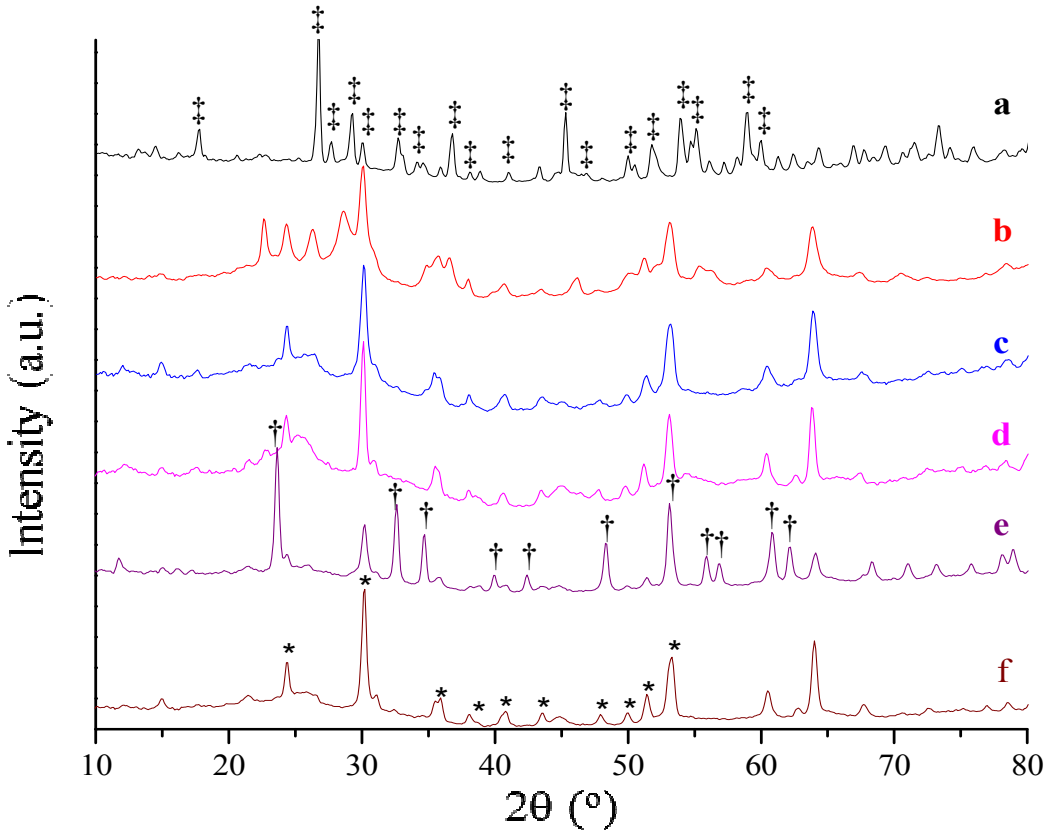

Figure S4. PXRD of different copper(I)-niobates obtained from the solvothermal reaction (150 ^{o}C) between CuCl and Li_3NbO_4 nanoparticles at different molar ratios and heating times of a) 12:1 for 4days, b) 7:1 for 4 days, c) 5:1 for 5days, d) 4.5:1 for 5 days, e) 4:1 for 3days 16hr, and f) 4:1 for 4days 14hr. Each product was heated to 450 ^{o}C for 24 h after the solvothermal reaction. Note - ‡ = $Cu_2Nb_8O_{21}$, † = $Li_xCu_{1-x}NbO_3$ ($x < 1$), and * = $Li_xCu_{1-x}Nb_3O_8$.

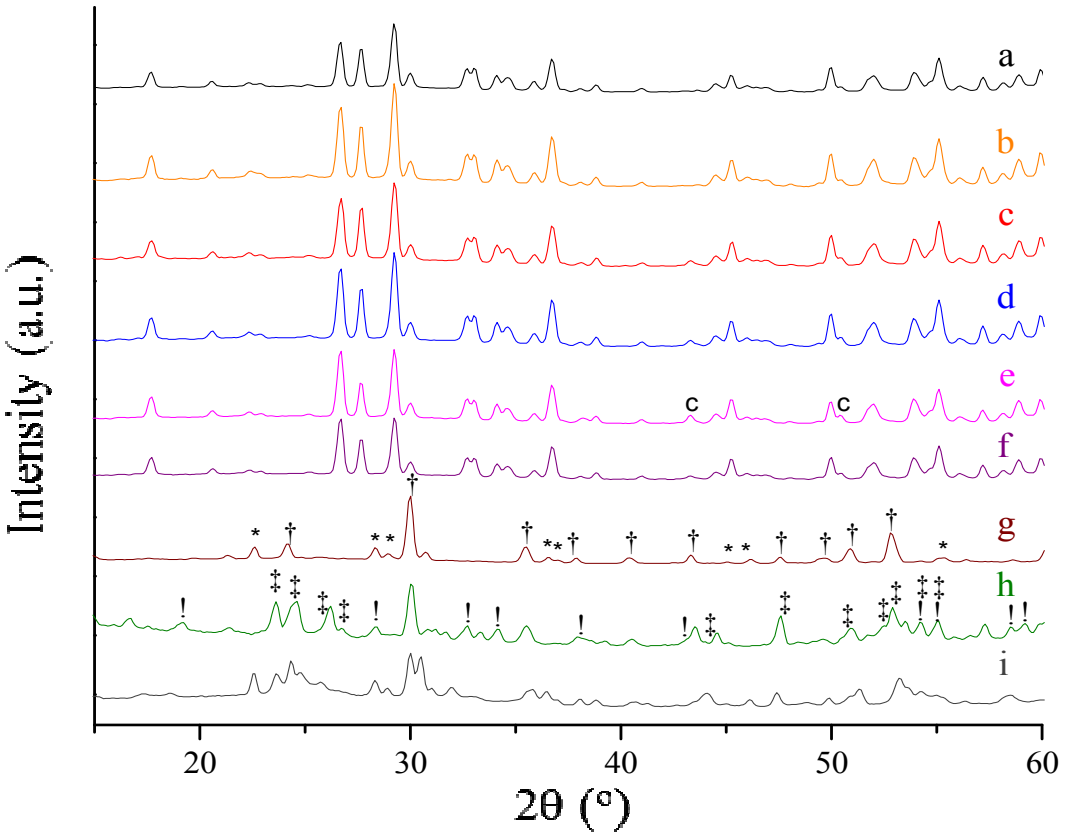

Figure S5. PXRD plots of micron-sized $Cu_2Nb_8O_{21}$ particles after a) non-heat treated, and after heating under N_2 gas at b) 250 °C, c) 300 °C, d) 400 °C, e) 500 °C, f) 600 °C, g) 750 °C, h) 1000 °C after drying at 200 °C for 3hr, and i) 750 °C rapid heating. Note: C = Cu (JCPDS # 4-836), * = Nb_2O_5(JCPDS # 27-1313), † = $CuNb_3O_8$ (JCPDS # 1-71-1927), ! = $CuNbO_3$(ICSD-PDF # 97-020-1899), ‡ = $Nb_{12}O_{29}$ (JCPDS # 1-73-1610)

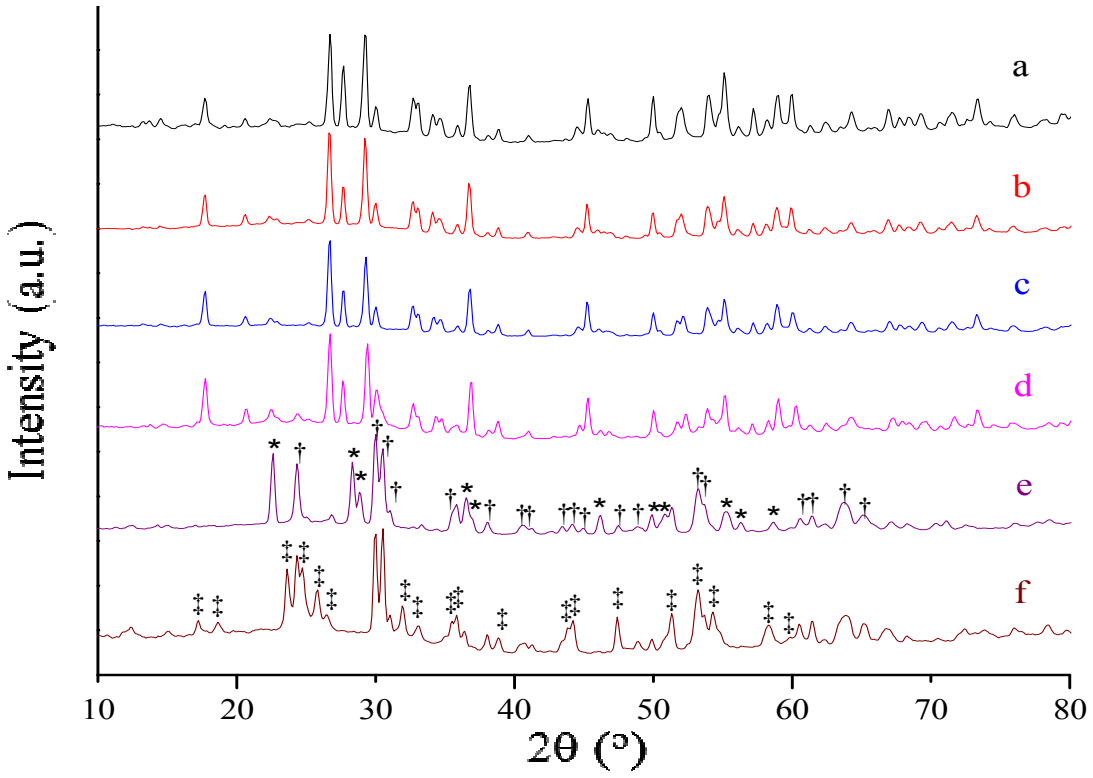

Figure S6. PXRD plots of $Cu_2Nb_8O_{21}$ nanoparticles (1h reaction) after heating in air to a) 200 °C, b) 300 °C, c) 400 °C, d) 600 °C, e) 750 °C, and f) 900 °C. Note: * = Nb_2O_5(JCPDS # 27-1313), † = $CuNb_2O_6$(JCPDS # 45-561), and ‡ = $Nb_{12}O_{29}$ (JCPDS # 1-73-1610)

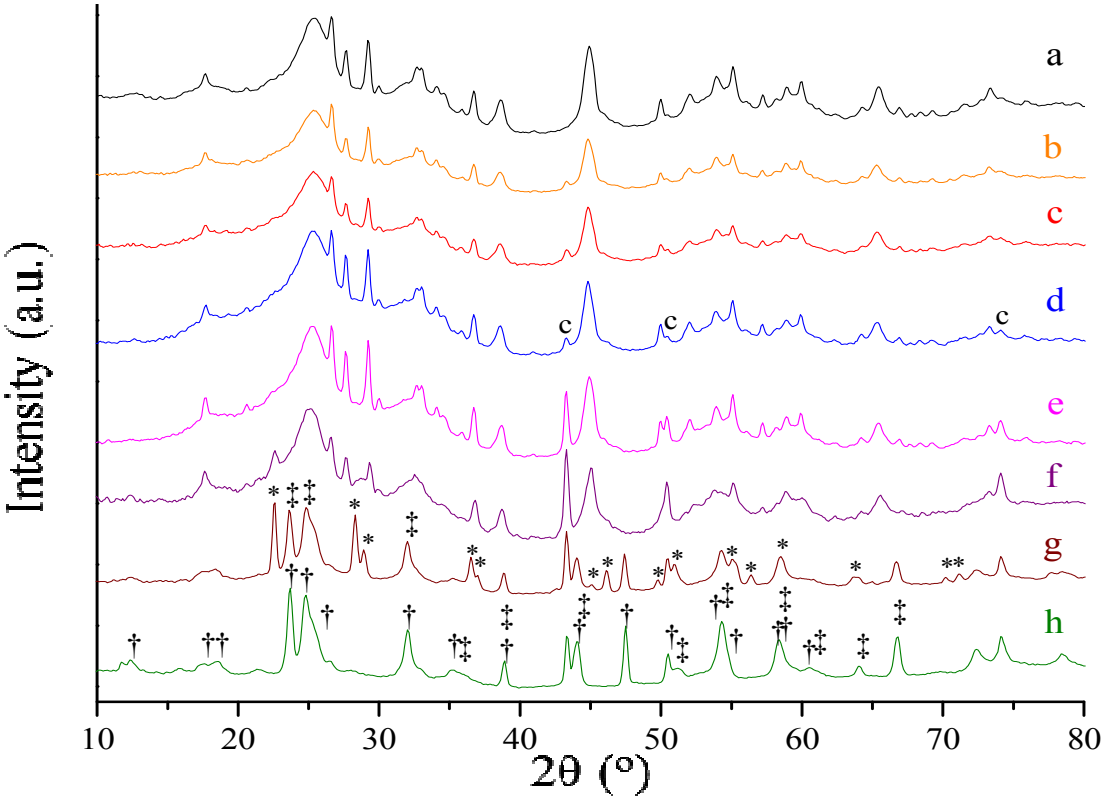

Figure S7. PXRD plots of $Cu_2Nb_8O_{21}$ nanoparticles (30 min reaction) after a) non heating, and after heating under N_2 at b) 250 °C, c) 300 °C, d) 400 °C, e) 500 °C, f) 600 °C, g) 750 °C, and h) 1000 °C. Note: c = Cu (JCPDS # 4-836), * = Nb_2O_5 (JCPDS # 27-1313), † = $Nb_{12}O_{29}$ (JCPDS # 1-73-1610), ‡ = Nb_2O_5 (JCPDS # 15-166)

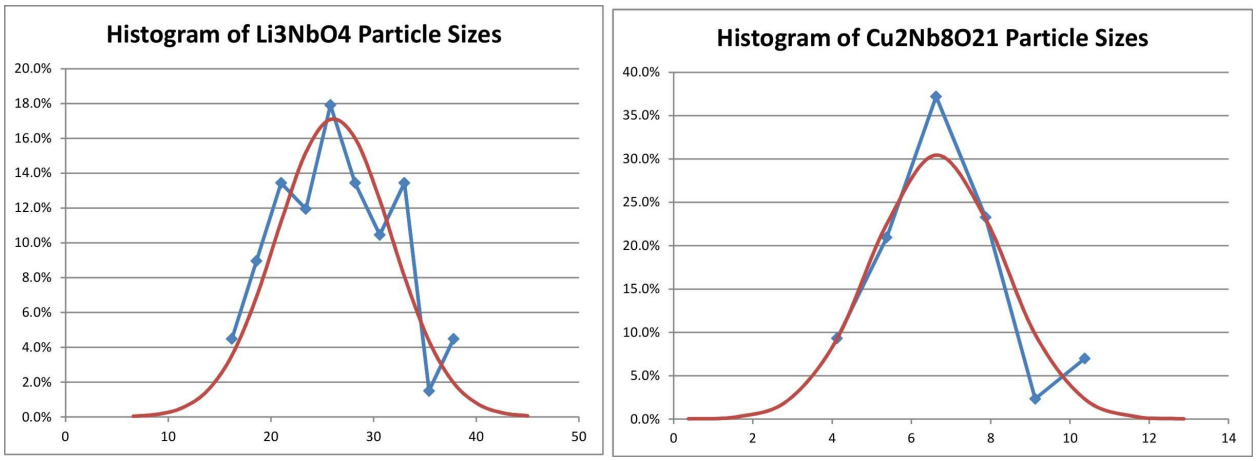

Figure S8. Histrograms of particle sizes for multi-pored Li_3NbO_4 nanoparticles (left) and $Cu_2Nb_8O_{21}$ nanoparticles (right) for a 30 min reaction time.

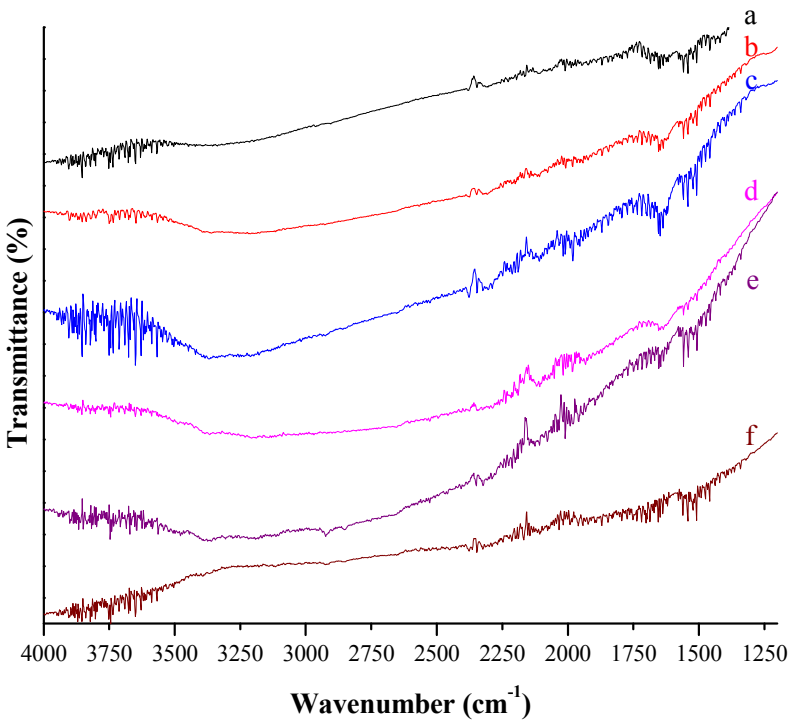

Figure S9. FT-IR plots of a) washed and well-dried product at 450 ^oC for 30minute, b) heat treated at 300 ^oC, c) 400 ^oC, d) 500 ^oC, e) 600 ^oC, and f) at 750 ^oC under N_2 gas.

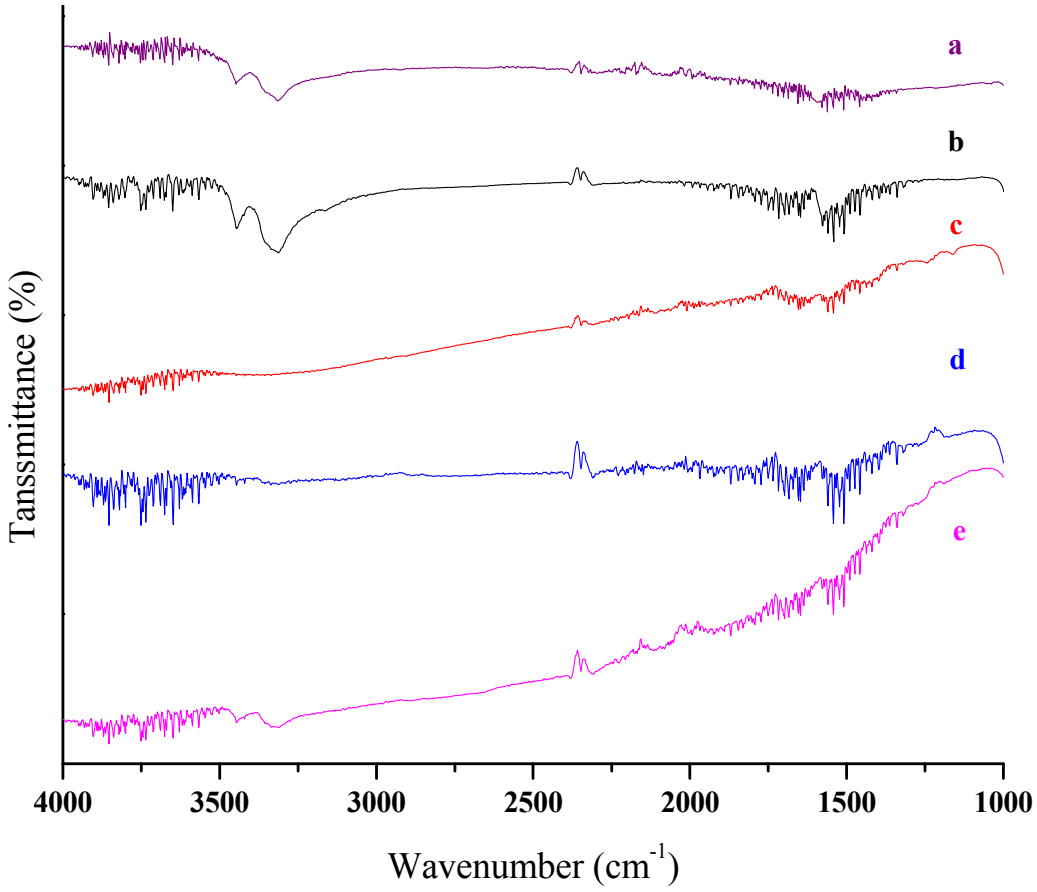

Figure S10. FT-IR plots of a) dried CuCl (Alfa Aesar), b) as-synthesized $Cu_2Nb_8O_{21}$ products, c) washed and well-dried product at 400 ^oC for 30minute, and, d) and e), heat treated c at 500 ^oC, and 650 ^oC in vacuum sealed quartz tube for 1 day, respectively.

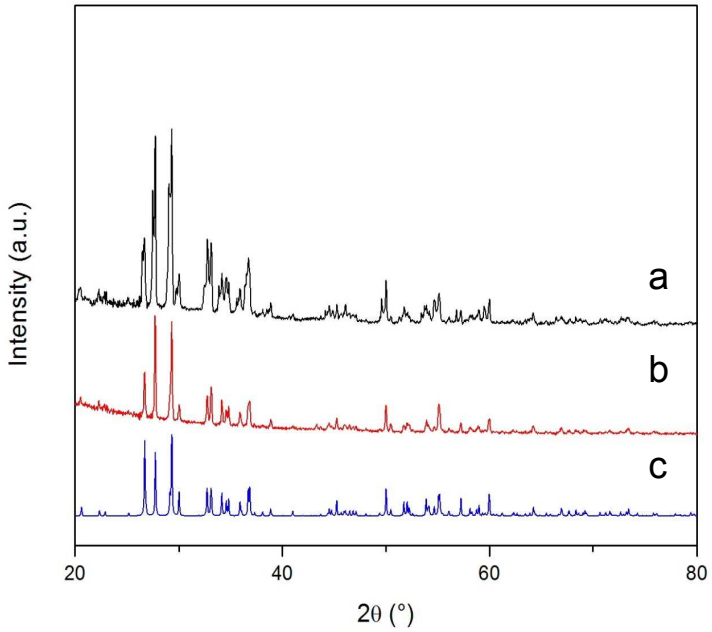

Figure S11. The PXRD patterns of $Cu_2Nb_8O_{21}$ polycrystalline films after annealing at 500 °C under vacuum (not heated in air) and both before (a) and after (b) the voltammetric scans at a pH of 12, and c) calculated PXRD pattern.

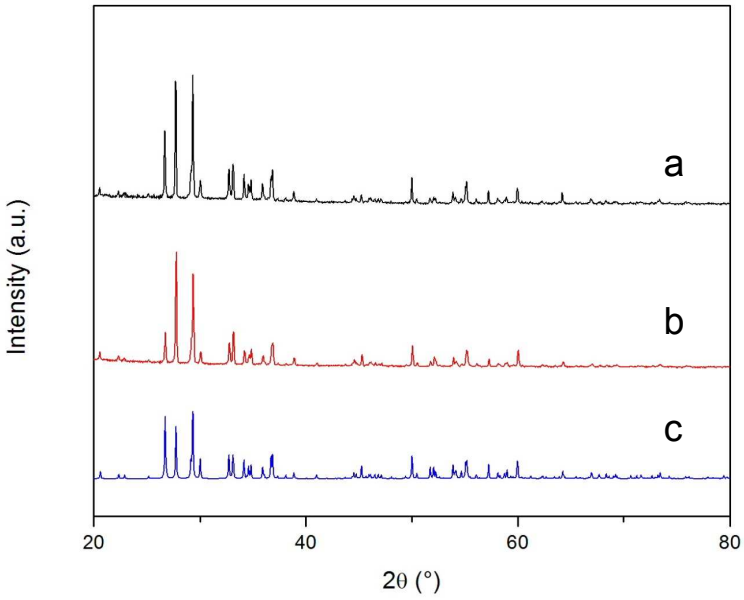

Figure S12. The PXRD patterns of $Cu_2Nb_8O_{21}$ polycrystalline films after annealing at 500 °C under vacuum, followed by heating air 350 °C for 3 h, a) after cyclic voltammetric scans at a pH of 12, b) before the cyclic voltammetric scans, and c) the calculated PXRD pattern.

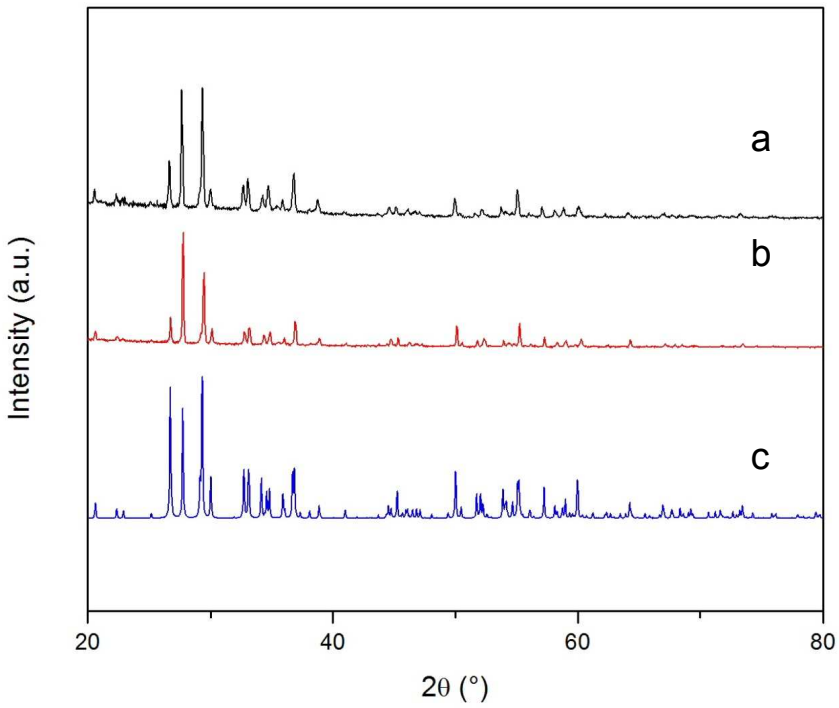

Figure S13. The PXRD pattern of $Cu_2Nb_8O_{21}$ polycrystalline films after annealing at 500 °C under vacuum, followed by heating in air at 450 °C for 3 h, and a) after cyclic voltammetric scans at a pH of 12, b) before cyclic voltammetric scans, and c) the calculated PXRD pattern.